

Transformer-based Learning-to-Optimize Approach for Scalable and Generalizable Beamforming

Yubo Zhang, Xiao-Yang Liu, and Xiaodong Wang

Abstract— We develop an unsupervised deep learning framework for downlink beamforming in large-scale MU-MISO channels. The model is trained offline, allowing real-time inference through lightweight feedforward computations in dynamic communication environments. Following the learning-to-optimize (L2O) paradigm, a multi-layer Transformer iteratively refines both channel and beamformer features via residual connections. To enhance training, three strategies are introduced: (i) curriculum learning (CL) to improve early-stage convergence and avoid local optima, (ii) semi-amortized learning to refine each Transformer block with a few gradient ascent steps, and (iii) sliding-window training to stabilize optimization by training only a subset of Transformer blocks at a time. Extensive simulations show that the proposed scheme outperforms existing baselines at low-to-medium SNRs and closely approaches WMMSE performance at high SNRs, while achieving substantially faster inference than iterative and online learning approaches.

Index Terms—Transformer model, deep residual learning, learning-to-optimize, downlink beamforming, semi-amortized learning, curriculum learning, sliding-window training

I. INTRODUCTION

Next-generation wireless communication systems are characterized by higher carrier frequencies and large-scale antenna arrays, which necessitate scalable architectures and low-latency processing designs. Among various physical-layer innovations, real-time downlink beamforming — where the base station (BS) continuously updates its transmit beamformers according to time-varying downlink channels — has become a key enabler of capacity-approaching transmission and has received considerable research attention. Conventional iterative algorithms, such as the weighted MMSE (WMMSE) method [1], can achieve near-optimal performance but are computationally prohibitive for large-scale systems. In contrast, low-complexity schemes such as maximum ratio transmission (MRT) [2] and LMMSE beamforming [3] offer fast solutions at the cost of significant performance degradation. Recently, deep learning (DL)-based approaches, particularly Transformer networks, have been investigated to achieve high-quality beamformer solutions with improved scalability and real-time adaptability.

Early studies attempted to directly learn the mapping from input features to beamformer solutions. In [4], a deep neural network (DNN) was employed to approximate the channel state information (CSI)-to-beamformer mapping in a supervised data-driven manner. The work in [5] predicted beamformer solutions from historical CSI using a convolutional long short term memory (LSTM) network. In [6], a ResNet-18

backbone was utilized to extract multi-modal sensing features, followed by a Transformer network to enhance beamforming learning. Furthermore, [7] proposed a deep encoder-decoder network (EDN) specifically designed for beamforming optimization under large-scale sparse channels, while [8] leveraged reflected signal echoes and adopted a CNN-Transformer architecture for predictive beamforming in integrated sensing and communication (ISAC) systems. In addition, the authors of [9] employed a U-Net to extract latent channel features and subsequently used a Transformer network to generate various beamformer solutions under near-field scenarios.

Given the challenges of directly learning the beamforming mapping, another line of research focuses on decomposing the beamforming task into multiple optimization steps, thereby reducing learning difficulty. In [10], a deep-unfolded WMMSE model was proposed to perform multi-step beamforming optimization with significantly lower complexity than the conventional WMMSE algorithm. By leveraging the learning to optimize (L2O) framework [11] and the curriculum learning (CL) strategy [12], the work in [13] developed an L2O-based bi-directional convolutional NN (BiCNN) architecture for beamforming optimization, which, however, exhibits degraded performance as the problem size increases. The study in [14] introduced a hierarchical permutation equivariance (HPE) Transformer for multicast beamforming under quality of Service (QoS) constraints, where the beamforming mapping is decomposed into multiple learning layers. Moreover, the authors in [15] employed a recurrent neural network (RNN)-based optimizer to directly learn beamformer gradients in a coordinate-wise manner, which performs well in the large-scale channels, albeit at the cost of considerable inference overhead.

To the best of our knowledge, none of the existing beamforming optimization schemes approach or surpass the WMMSE performance under very large-scale downlink channels while maintaining low inference overhead. To address this challenge, we develop a multi-layer Transformer network to implement a scalable L2O-based beamforming optimization scheme. The main contributions of this work are summarized as follows:

- Inspired by the learning-to-optimize paradigm, we design a multi-layer Transformer architecture tailored for downlink beamforming over large-scale Gaussian-sampled channels. Starting from the true channel and the corresponding LMMSE beamformer, both channel and beamformer features are iteratively refined through multiple Transformer blocks with residual connections.
- We incorporate amortized optimization [16] to shift the

Y. Zhang and X. Liu and X. Wang are with the Department of Electrical Engineering, Columbia University, New York, NY 10027.

computational burden from the online inference stage to offline training stage, making the proposed scheme suitable for real-time deployment. To further stabilize and accelerate training, we adopt the objective CL strategy and introduce a sliding-window training mechanism to ensure smooth optimization across multiple Transformer layers.

- Extensive simulations demonstrate both the training convergence and the testing performance of the proposed framework. Ablation studies validate the contribution of each training component. The results show that the proposed beamforming scheme outperforms multiple baselines, including the conventional WMMSE algorithm, under various SNR regimes and very large-scale system configurations, while incurring low inference latency.

II. SYSTEM DESCRIPTION AND PROBLEM FORMULATION

In this section, we introduce the downlink beamforming system model under a Gaussian channel assumption, and subsequently formulate an amortized beamforming optimization problem within the L2O framework.

A. System Description

We consider a single-cell downlink multiple-input-single-output (MISO) beamforming system, where a BS is equipped with an antenna array of size N_m arranged as a uniform linear array (ULA) with half-wavelength spacing. The maximum number of single-antenna users supported within the cell is denoted by K_m . We assume a time division duplex (TDD) transmission mode and adopt a Gaussian channel model. In practice, users may dynamically enter and leave the serving cell, such that the instantaneous number of active users satisfies $K \leq K_m$. Moreover, energy-efficient antenna selection strategies can be employed at the BS to reduce power consumption [17], resulting in an instantaneous number of activated antennas $N \leq N_m$. Consequently, the channel matrix between the activated antennas and the served users is denoted by $\mathbf{H} \in \mathbb{C}^{K \times N}$, whose entries are independently drawn as

$$[\mathbf{H}]_{ij} \stackrel{\text{i.i.d.}}{\sim} \mathcal{CN}(0, 1), \quad i \in [K], j \in [N], \quad (1)$$

which leads to $\mathbb{E}[\|\mathbf{H}\|_F^2] = KN$. Perfect CSI is assumed to be available at the BS. Let the channel vector between the BS and user k be denoted by $\mathbf{h}_k^T \in \mathbb{C}^{1 \times N}$. The BS applies a beamforming vector $\mathbf{w}_k \in \mathbb{C}^{N \times 1}$ to transmit the data symbol $x_k \in \mathbb{C}$ intended for user k . The received signal at user k can then be expressed as

$$y_k = \mathbf{h}_k^H \sum_{i=1}^K \mathbf{w}_i x_i + n_k, \quad (2)$$

where $n_k \sim \mathcal{CN}(0, \sigma_k^2)$ denotes the additive noise at user k . Define the overall channel matrix as $\mathbf{H} = [\mathbf{h}_1, \dots, \mathbf{h}_K]^T \in \mathbb{C}^{K \times N}$, and the beamforming matrix as $\mathbf{W} = [\mathbf{w}_1, \dots, \mathbf{w}_K] \in \mathbb{C}^{N \times K}$. The achievable sum rate in this MISO setting is given by

$$R_{\text{sum}}(\mathbf{H}, \mathbf{W}) = \sum_{k=1}^K \log_2 \left(1 + \frac{|\mathbf{h}_k^H \mathbf{w}_k|^2}{\sigma_k^2 + \sum_{i \neq k} |\mathbf{h}_k^H \mathbf{w}_i|^2} \right), \quad (3)$$

Concretely, a downlink MISO system where the number of served users is smaller than that of the activated antenna, i.e., $K < N$, is referred to as an underloaded system. Correspondingly, downlink MISO systems with $K = N$ and $K > N$ are referred to as a critically-loaded system and an overloaded system, respectively. In general, achieving high-rate beamformer solutions in overloaded systems is more challenging than in underloaded or critically loaded systems [18], since linear precoding schemes are no longer capable of effectively suppressing inter-user interference (IUI) in this regime.

B. Problem Formulation

According to (1) and (3), we define $\mathcal{S}^{K \times N}$ as the entire state space of Gaussian-sampled channel matrices of dimension $K \times N$, where $K \in [K_m]$ and $N \in [N_m]$. Our objective is then described by the following family of optimization problems:

$$\forall (K, N) \in [K_m] \times [N_m], \text{ and } \forall \mathbf{H} \in \mathcal{S}^{K \times N} : \\ \max_{\mathbf{W} \in \mathbb{C}^{N \times K}} R_{\text{sum}}(\mathbf{H}, \mathbf{W}), \quad \|\mathbf{W}\|_F^2 \leq P, \quad (4)$$

where $R_{\text{sum}} : \mathcal{S}^{K \times N} \times \mathbb{C}^{N \times K} \rightarrow \mathbb{R}$ is the sum-rate objective defined in (3). Directly learning the optimal beamforming mapping $\mathbf{W}^*(\mathbf{H}) = \arg \max_{\mathbf{W} \in \mathbb{C}^{N \times K}} R_{\text{sum}}(\mathbf{H}, \mathbf{W})$ for all channel realizations $\mathbf{H} \in \mathcal{S}^{K \times N}$ and all possible values of (K, N) is highly challenging, since the beamforming optimization problem is in general NP-hard. Alternatively, we adopt the L2O approach to obtain near-optimal beamformer solutions, which mitigates this difficulty by amortizing the optimization task to each learnable optimization step [11]. Specifically, for a given channel realization $\mathbf{H} \in \mathcal{S}^{K \times N}$, the corresponding LMMSE beamformer $\mathbf{W}^{(0)} = [\mathbf{w}_1^{(0)}, \dots, \mathbf{w}_K^{(0)}]$ is chosen as the initial input to the first optimization block, and is computed as

$$\mathbf{w}_k^{(0)} = \sqrt{\frac{P}{K}} \cdot \frac{(\mathbf{I}_N + \sum_{i=1}^K \frac{P}{K} \mathbf{h}_i \mathbf{h}_i^H)^{-1} \mathbf{h}_k}{\|(\mathbf{I}_N + \sum_{i=1}^K \frac{P}{K} \mathbf{h}_i \mathbf{h}_i^H)^{-1} \mathbf{h}_k\|_2}, \quad k \in [K]. \quad (5)$$

To enhance the model expressivity, we consider an L2O framework in which the parameters of the optimizer network are allowed to vary across layers. In particular, we denote the optimizer network at the t^{th} layer by \mathcal{F}_{θ_t} , where θ_t represents the learnable parameters and $t \in [T]$. The auxiliary variable and the solution are jointly fed into the network and updated as follows

$$\mathbf{H}^{(t)}, \mathbf{W}^{(t)} = \mathcal{F}_{\theta_t}(\mathbf{H}^{(t-1)}, \mathbf{W}^{(t-1)}), \quad (6)$$

where the initial auxiliary variable is the true channel, i.e., $\mathbf{H}^{(0)} = \mathbf{H}$, and the initial solution $\mathbf{W}^{(0)}$ is the corresponding LMMSE beamformer computed by (5). Notably, different from prior L2O designs that keep the state fixed across layers [13], our design enlarges the effective feature space for optimization by updating the auxiliary variable at each layer. From a kernel-method perspective, such representation lifting enhances the model expressivity and facilitates the discovery of higher-quality beamformer solutions.

Based on (6), to encourage performance improvement at every optimization step rather than focusing solely on the

final objective value, we maximize the cumulative sum-rate along the optimization trajectory. Accordingly, the original optimization formulation in (4) is reformulated as the following amortized learning problem:

$$\begin{aligned} & \forall (K, N) \in [K_m] \times [N_m] : \\ & \max_{\{\boldsymbol{\theta}_t\}_{t=1}^T} \mathbb{E}_{\mathbf{H} \in \mathcal{S}^{K \times N}} \left[\sum_{t=1}^T R_{\text{sum}}(\mathbf{H}, \mathbf{W}^{(t)}) \right], \\ & \text{s.t. } \|\mathbf{W}^{(t)}\|_F^2 \leq P, t \in [T], \end{aligned} \quad (7)$$

where $\{\mathbf{W}^{(t)}\}_{t=1}^T$ are generated according to (6). By learning the optimizer network parameters $\{\boldsymbol{\theta}_t\}_{t=1}^T$, the cost of the optimization is amortized over the training distribution, shifting the computational burden from online optimization in (4) to offline learning in (7). Nevertheless, solving (7) remains challenging for the following two reasons: (a) non-convex sum-rate maximization in large-scale systems is inherently difficult and lacks a general-purpose solver, and (b) the optimizer network is required to generalize across optimizers with different system configurations without re-training, including the overloaded cases which are intrinsically hard to optimize. In the following sections, we propose several novel architectural designs and training strategies to address these challenges in (7).

III. MASKED TRANSFORMER MODEL FOR BEAMFORMING OPTIMIZATION

A. Transformer-based SAO Framework

An semi-amortized learning-to-optimize (SAO) framework tailored to the problem in (7) is proposed, which leverages the semi-amortized learning paradigm [19] to further refine the beamformer solution by performing a few steps of gradient ascent following each optimizer network. Specifically, let $\mathbf{W}_0^{(t)}$ denote the beamformer output produced by the optimizer network at the t^{th} layer. The refined beamformer is then given by $\mathbf{W}^{(t)} \triangleq \mathbf{W}_Q^{(t)} \triangleq \mathcal{G}_Q(\mathbf{W}_0^{(t)})$, which is obtained as follows:

$$\begin{aligned} \mathbf{W}_q^{(t)} &= \mathbf{W}_{q-1}^{(t)} + \eta_w \cdot \nabla_{\mathbf{W}} R_{\text{sum}}(\mathbf{H}, \mathbf{W}_{q-1}^{(t)}), \\ \mathbf{W}_q^{(t)} &= \sqrt{P} \cdot \frac{\mathbf{W}_q^{(t)}}{\|\mathbf{W}_q^{(t)}\|_F}, q \in [Q]. \end{aligned} \quad (8)$$

As discussed in [20], optimizing residual mappings rather than the original unreferenced mappings facilitates stable training of deep networks. Accordingly, at the t^{th} layer, the optimizer network $\mathcal{F}_{\boldsymbol{\theta}_t}(\mathbf{H}^{(t-1)}, \mathbf{W}^{(t-1)})$ is trained to approximate the residuals $\Delta \mathbf{W}_0^{(t)} \triangleq \mathbf{W}_0^{(t)} - \mathbf{W}^{(t-1)}$ and $\Delta \mathbf{H}^{(t)} \triangleq \mathbf{H}^{(t)} - \mathbf{H}^{(t-1)}$, i.e.,

$$\Delta \mathbf{H}^{(t)}, \Delta \mathbf{W}_0^{(t)} = \mathcal{F}_{\boldsymbol{\theta}_t}(\mathbf{H}^{(t-1)}, \mathbf{W}^{(t-1)}). \quad (9)$$

Hence, the forward process in (6) can be reformulated as follows:

$$\begin{aligned} \mathbf{H}^{(t)} &= \mathbf{H}^{(t-1)} + \mathcal{F}_{\boldsymbol{\theta}_t}(\mathbf{H}^{(t-1)}, \mathbf{W}^{(t-1)})[0], \\ \mathbf{W}^{(t)} &= \mathcal{G}_Q(\mathbf{W}^{(t-1)} + \mathcal{F}_{\boldsymbol{\theta}_t}(\mathbf{H}^{(t-1)}, \mathbf{W}^{(t-1)})[1]), \end{aligned} \quad (10)$$

for $t \in [T]$.

Remark 1. Based on (10), a simplified model can be constructed in which the auxiliary variable is fixed as the true channel across all L2O layers. Specifically, only the beamformer solution is updated at the t^{th} layer, given by

$$\Delta \mathbf{W}_0^{(t)} = \mathcal{F}_{\boldsymbol{\theta}_t}(\mathbf{H}, \mathbf{W}^{(t-1)}), \mathbf{W}^{(t)} = \mathcal{G}_Q(\mathbf{W}^{(t-1)} + \Delta \mathbf{W}_0^{(t)}). \quad (11)$$

This setting reduces the computational burden, at the expense of a reduced model expressivity, since the inputs to all layers are confined to a narrower feature space due to the fixed auxiliary variable. For clarity, we refer to the simplified model in (11) as the *SAO* model. In contrast, the model in (10) is termed the *SAO-lift* model, as it performs representation lifting by updating the auxiliary variable at each layer.

A block diagram of the SAO-lift model is illustrated in Fig. 1. The SAO model follows a similar architecture, except that the auxiliary variable \mathbf{H} remains unchanged across layers. Unless otherwise specified, we focus on the SAO-lift model in the sequel.

B. Masked Transformer Architecture

To achieve near-optimal beamformer solutions, we adopt Transformers to parameterize the optimizer networks $\{\mathcal{F}_{\boldsymbol{\theta}_t}\}_{t=1}^T$ in Fig. 1, motivated by their strong scalability to large-scale systems and state-of-the-art expressive power. In addition, the residual connections inherent in Transformer architectures facilitate stable training of deep networks, which aligns well with the proposed optimization framework in Fig. 1.

In this work, we further aim to learn a single Transformer model with fixed input and output dimensions that can produce high-quality beamformer solutions across varying user-antenna configurations. This objective poses a significant challenge for vanilla Transformers, which do not inherently exhibit two-dimensional size-generalizability [21]. To address this challenge, inspired by prior successful applications of masking operations [22], [23], we propose a masked Transformer architecture tailored to dynamic downlink systems. The key idea is to apply a structured scheduling of antenna-user masking during training, enabling a single model to be trained on channel samples with heterogeneous system configurations. This strategy allows the model to capture a more complex underlying data distribution and substantially improves its generalizability.

1) *Sample Masking:* To proceed, we first obtain a sample masking matrix $\mathbf{M}_s \in \{0, 1\}^{K_m \times N_m}$ based on the true channel matrix $\mathbf{H} \in \mathbb{C}^{K_m \times N_m}$. Let $\mathbf{R}_u \subseteq \{1, \dots, K_m\}$ and $\mathbf{R}_a \subseteq \{1, \dots, N_m\}$ denote the index sets of the masked (out-of-cell) users and of the masked (deactivated) antennas, respectively. In practice, these index sets can be determined by identifying user-level and antenna-level channel vectors in \mathbf{H} with significantly weaker channel strengths during inference.

Given \mathbf{R}_u and \mathbf{R}_a , the sample masking matrix \mathbf{M}_s is constructed to remove the channel entries associated with

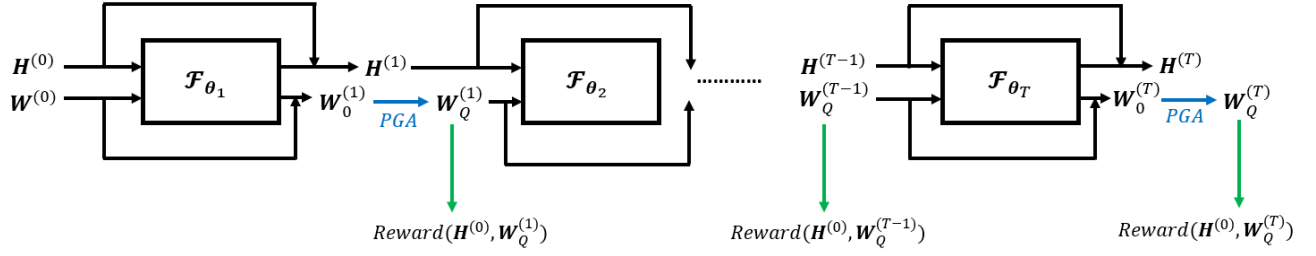


Fig. 1: SAO-lift model for beamforming optimization.

masked users and antennas in a Hadamard-product manner, defined as

$$M_s(k, n) = \begin{cases} 0, & k \in \mathbf{R}_u \text{ or } n \in \mathbf{R}_a, \\ 1, & \text{otherwise.} \end{cases} \quad (12)$$

The input channel to the first layer is then obtained as $\mathbf{H}^{(0)} = \mathbf{H} \circ M_s$. Accordingly, the input beamformer $\mathbf{W}^{(0)}$ is initialized as the LMMSE beamformer computed based on the masked channel matrix $\mathbf{H}^{(0)}$.

2) *Token Sequence Construction*: We then construct the token sequences based on the inputs to each layer. Let $(\mathbf{H}_{\text{in}}, \mathbf{W}_{\text{in}})$ denote the channel and beamformer inputs, respectively. Each of $\mathbf{H}_{\text{in}} \in \mathbb{C}^{K_m \times N_m}$ and $\mathbf{W}_{\text{in}} \in \mathbb{C}^{K_m \times N_m}$ can be interpreted as a sequence of antenna-level vectors, i.e., $\mathbf{H}_{\text{in}} = [\mathbf{h}_1, \dots, \mathbf{h}_{N_m}]$ and $\mathbf{W}_{\text{in}} = [\mathbf{w}_1, \dots, \mathbf{w}_{N_m}]$. For each antenna-level channel vector $\mathbf{h}_n \in \mathbb{C}^{K_m}$, the real and imaginary components are separated and concatenated as $\mathbf{h}_n^{(a)} = [\mathcal{R}(\mathbf{h}_n); \mathcal{I}(\mathbf{h}_n)] \in \mathbb{R}^{2K_m}$, yielding the real-valued antenna-level channel matrix $\mathbf{H}_a = [\mathbf{h}_1^{(a)}, \dots, \mathbf{h}_{N_m}^{(a)}] \in \mathbb{R}^{2K_m \times N_m}$. Similarly, for each antenna-level beamformer vector $\mathbf{w}_n \in \mathbb{C}^{K_m}$, we obtain $\mathbf{w}_n^{(a)} = [\mathcal{R}(\mathbf{w}_n); \mathcal{I}(\mathbf{w}_n)] \in \mathbb{R}^{2K_m}$, and form the real-valued antenna-level beamformer matrix $\mathbf{W}_a = [\mathbf{w}_1^{(a)}, \dots, \mathbf{w}_{N_m}^{(a)}] \in \mathbb{R}^{2K_m \times N_m}$. Likewise, the transposed inputs $\mathbf{H}_{\text{in}}^T \in \mathbb{C}^{N_m \times K_m}$ and $\mathbf{W}_{\text{in}}^T \in \mathbb{C}^{N_m \times K_m}$ can be viewed as sequences of user-level vectors, i.e., $\mathbf{H}_{\text{in}}^T = [\mathbf{h}_1, \dots, \mathbf{h}_{K_m}]$ and $\mathbf{W}_{\text{in}}^T = [\mathbf{w}_1, \dots, \mathbf{w}_{K_m}]$. For each user-level channel vector $\mathbf{h}_k \in \mathbb{C}^{N_m}$, we define $\mathbf{h}_k^{(u)} = [\mathcal{R}(\mathbf{h}_k); \mathcal{I}(\mathbf{h}_k)] \in \mathbb{R}^{2N_m}$, which yields the real-valued user-level channel matrix $\mathbf{H}_u = [\mathbf{h}_1^{(u)}, \dots, \mathbf{h}_{K_m}^{(u)}] \in \mathbb{R}^{2N_m \times K_m}$. The real-valued user-level beamformer matrix $\mathbf{W}_u = [\mathbf{w}_1^{(u)}, \dots, \mathbf{w}_{K_m}^{(u)}] \in \mathbb{R}^{2N_m \times K_m}$ is constructed in the same manner. The antenna-level and user-level token sequences are then formed as

$$\mathbf{S} = [\mathbf{H}_u, \mathbf{W}_u] \in \mathbb{R}^{2N_m \times 2K_m}, \quad \mathbf{T} = [\mathbf{H}_a, \mathbf{W}_a] \in \mathbb{R}^{2K_m \times 2N_m}. \quad (13)$$

For notational convenience, we set $K_m = N_m = L$ throughout this paper. Consequently, each token has dimension $2L$, and the corresponding sequence length is also $2L$.

Next, the sequences \mathbf{S} and \mathbf{T} are processed independently by two embedding layers. Each embedding layer consists of a fully-connected (FC) layer followed by a token-wise normalization (TN) layer. Given input tokens of dimension $2L$, the

FC layer projects them into an M -dimensional space, yielding $\tilde{\mathbf{S}} \in \mathbb{R}^{M \times 2L}$ and $\tilde{\mathbf{T}} \in \mathbb{R}^{M \times 2L}$. The subsequent TN layers normalize each token independently, producing the normalized embeddings $\bar{\mathbf{S}}$ and $\bar{\mathbf{T}}$. Importantly, no positional encoding is applied, as it would compromise the model's permutation equivariance (PE) property under dynamic scenarios.

3) *Multi-head Self-attention with Attention Masking*: The multi-head self-attention (MHSA) scheme employs multiple attention heads to project the embedded tokens into distinct subspaces, thereby capturing diverse interaction patterns while improving training stability and generalization. Specifically, for the e^{th} attention head, the query, key, and value matrices corresponding to the user-level sequence $\bar{\mathbf{S}}$ are obtained as

$$\mathbf{Q}_s^e = \bar{\mathbf{S}}^T \mathbf{Z}_Q^e, \quad \mathbf{K}_s^e = \bar{\mathbf{S}}^T \mathbf{Z}_K^e, \quad \mathbf{V}_s^e = \bar{\mathbf{S}}^T \mathbf{Z}_V^e, \quad (14)$$

where $\mathbf{Z}_Q^e, \mathbf{Z}_K^e, \mathbf{Z}_V^e \in \mathbb{R}^{M \times D_e}$ are the learnable query, key, and value projection matrices, respectively. Similarly, for the antenna-level sequence $\bar{\mathbf{T}}$, the projected matrices are given by

$$\mathbf{Q}_t^e = \bar{\mathbf{T}}^T \mathbf{X}_Q^e, \quad \mathbf{K}_t^e = \bar{\mathbf{T}}^T \mathbf{X}_K^e, \quad \mathbf{V}_t^e = \bar{\mathbf{T}}^T \mathbf{X}_V^e, \quad (15)$$

with $\mathbf{X}_Q^e, \mathbf{X}_K^e, \mathbf{X}_V^e \in \mathbb{R}^{M \times D_e}$ being the corresponding learnable projection matrices.

To prevent attention from being diffused over masked users or antennas, we construct the attention masking matrices $\mathbf{M}_U \in \mathbb{R}^{2L \times 2L}$ and $\mathbf{M}_A \in \mathbb{R}^{2L \times 2L}$ based on the sample masking matrix M_s . These masks are added to the user-level and antenna-level attention score matrices, respectively. Specifically, we have

$$\mathbf{M}_U = [\mathbf{M}_u, \mathbf{M}_u; \mathbf{M}_u, \mathbf{M}_u], \quad \mathbf{M}_A = [\mathbf{M}_a, \mathbf{M}_a; \mathbf{M}_a, \mathbf{M}_a], \quad (16)$$

where

$$\mathbf{M}_u(i, j) = \begin{cases} -\infty, & i \in \mathbf{R}_u \text{ or } j \in \mathbf{R}_u, \\ 0, & \text{otherwise,} \end{cases} \quad (17)$$

and

$$\mathbf{M}_a(i, j) = \begin{cases} -\infty, & i \in \mathbf{R}_a \text{ or } j \in \mathbf{R}_a, \\ 0, & \text{otherwise.} \end{cases} \quad (18)$$

Note that the block-wise partitioning in (16) arises from the joint inclusion of channel vectors and beamformer vectors

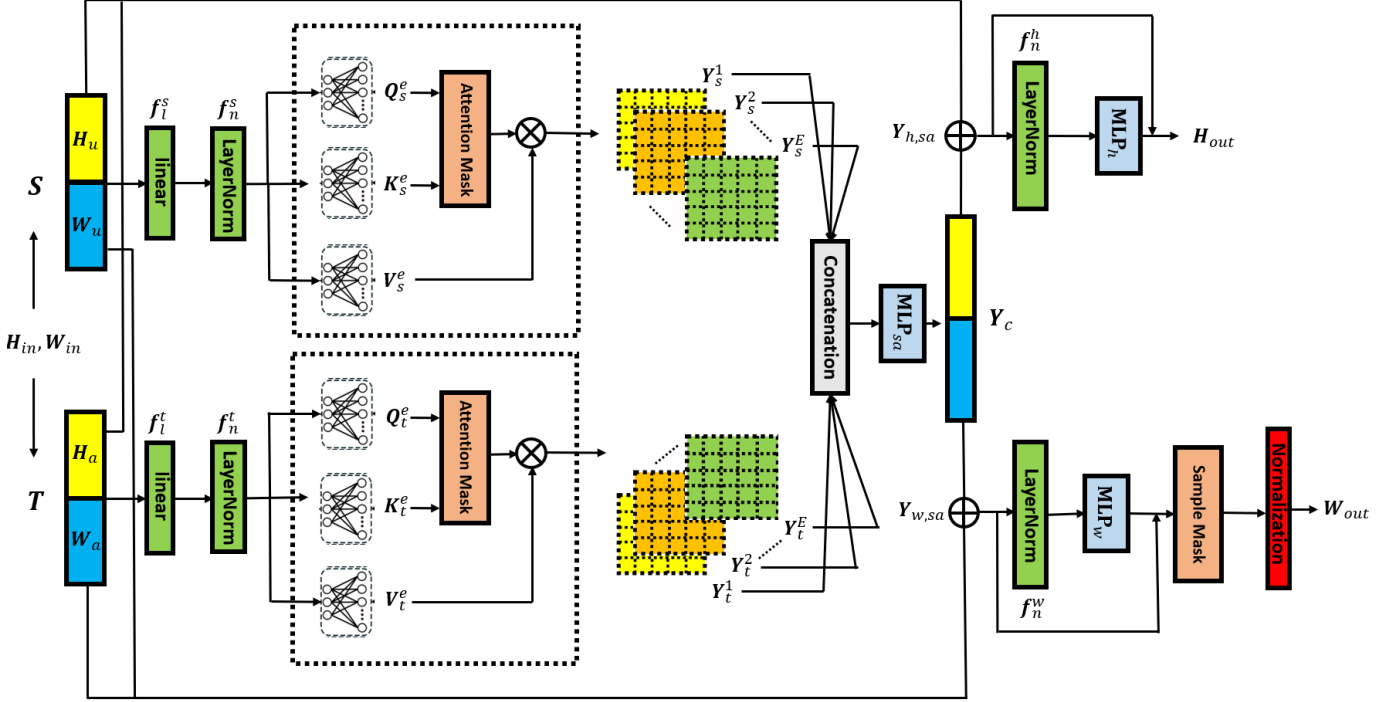


Fig. 2: The architecture of each Transformer layer.

in the token construction. The user-level and antenna-level attention logits are computed as

$$\begin{aligned} \mathbf{Y}_s^e &= \text{softmax} \left(\frac{\mathbf{Q}_s^e (\mathbf{K}_s^e)^T}{\sqrt{D_e}} + \mathbf{M}_U \right) \mathbf{V}_s^e, \quad e \in [E], \\ \mathbf{Y}_t^e &= \text{softmax} \left(\frac{\mathbf{Q}_t^e (\mathbf{K}_t^e)^T}{\sqrt{D_e}} + \mathbf{M}_A \right) \mathbf{V}_t^e, \quad e \in [E], \end{aligned} \quad (19)$$

such that all attention scores associated with masked users or masked antennas are assigned $-\infty$ and are therefore nullified after the Softmax operation.

The results in (19) are then concatenated to form

$$\mathbf{Y} = [\mathbf{Y}_s^1, \dots, \mathbf{Y}_s^E, \mathbf{Y}_t^1, \dots, \mathbf{Y}_t^E]^T \in \mathbb{R}^{D \times 2L}, \quad (20)$$

where $D \triangleq 2D_e E$. To effectively aggregate the outputs from all attention heads, we apply a multi-layer perceptron (MLP) after the concatenation in (20), denoted by $\text{MLP}_{sa}(\cdot) : \mathbb{R}^D \rightarrow \mathbb{R}^{2L}$, which produces $\mathbf{Y}_c = \text{MLP}_{sa}(\mathbf{Y}) \in \mathbb{R}^{2L \times 2L}$. The MLP typically consists of an FC layer, a GELU activation layer, and a dropout layer, thereby enhancing the expressive power by introducing non-linearity into the multi-head aggregation process. By applying residual connections, the outputs of the MHSA component are obtained as

$$\begin{aligned} \mathbf{Y}_{h,sa} &= \mathbf{Y}_c[:, 1:L] + \mathbf{S}[:, 1:L] + \mathbf{T}[:, 1:L], \\ \mathbf{Y}_{w,sa} &= \mathbf{Y}_c[:, L+1:2L] + \mathbf{S}[:, L+1:2L] + \mathbf{T}[:, L+1:2L], \end{aligned} \quad (21)$$

where the two segmented representations are subsequently fed into two separate MLP blocks for further processing.

4) *Output MLP*: This component outputs the updated auxiliary variable and beamformer solution via two dedicated MLP networks, denoted by $\text{MLP}_h(\cdot) : \mathbb{R}^{2L} \rightarrow \mathbb{R}^{2L}$ and $\text{MLP}_w(\cdot) : \mathbb{R}^{2L} \rightarrow \mathbb{R}^{2L}$, respectively. Specifically, the intermediate results in (21) are first normalized by TN layers, yielding $\bar{\mathbf{Y}}_{h,sa}$ and $\bar{\mathbf{Y}}_{w,sa}$. The normalized results are then fed into the corresponding MLP networks:

$$\bar{\mathbf{Y}}_{h,out} = \text{MLP}_h(\bar{\mathbf{Y}}_{h,sa}), \quad \bar{\mathbf{Y}}_{w,out} = \text{MLP}_w(\bar{\mathbf{Y}}_{w,sa}). \quad (22)$$

By incorporating residual connections, we have

$$\mathbf{Y}_{h,out} = \bar{\mathbf{Y}}_{h,out} + \mathbf{Y}_{h,sa}, \quad \mathbf{Y}_{w,out} = \bar{\mathbf{Y}}_{w,out} + \mathbf{Y}_{w,sa}. \quad (23)$$

We then combine the real and imaginary parts to recover the complex-valued matrices:

$$\begin{aligned} \mathbf{H}_{out} &= \mathbf{Y}_{h,out}[1:L] + j \cdot \mathbf{Y}_{h,out}[L+1:2L], \\ \bar{\mathbf{W}}_{out} &= \mathbf{Y}_{w,out}[1:L] + j \cdot \mathbf{Y}_{w,out}[L+1:2L]. \end{aligned} \quad (24)$$

To enforce the inactivity of masked users and antennas in the beamformer solution, we reapply the sample masking matrix, yielding $\mathbf{W}_{out} = \bar{\mathbf{W}}_{out} \circ \mathbf{M}_s$. The masked beamformer solution is then normalized to satisfy the transmit power constraint as $\mathbf{W}_{out} = \sqrt{P} \cdot \frac{\bar{\mathbf{W}}_{out}}{\|\bar{\mathbf{W}}_{out}\|_2}$. As a result, the masked Transformer at the t^{th} layer maps the input pair $(\mathbf{H}_{in}, \mathbf{W}_{in}) = (\mathbf{H}^{(t-1)}, \mathbf{W}^{(t-1)})$ to the output pair $(\mathbf{H}_{out}, \mathbf{W}_{out}) = (\mathbf{H}^{(t)}, \mathbf{W}_0^{(t)})$. Similar to (8), we further perform a Q -step gradient ascent refinement initialized at $\mathbf{W}_0^{(t)}$ based on the masked channel $\mathbf{H} \circ \mathbf{M}_s$, which outputs the refined beamformer solution $\mathbf{W}^{(t)} \triangleq \mathbf{W}_Q^{(t)}$.

In summary, the architecture of each layer of the masked Transformer is illustrated in Fig. 2. The key insight is that

the proposed masked Transformer can naturally accommodate varying activated antenna–user configurations through the joint use of adaptive sample masking and attention masking strategies.

C. Enhanced Training Methods

In this section, we present several novel techniques to improve the training convergence of the proposed masked-Transformer-based SAO-lift (MT-SAO-lift) model.

1) *Sliding-window Training Method*: The end-to-end training of the model in Fig. 1 becomes challenging when the episode length T is large, as backpropagating through all T layers simultaneously leads to unstable gradients and high memory consumption. To address these issues and reduce the computational cost during training, we adopt a sliding-window strategy inspired by truncated backpropagation through time (TBPTT) method in RNN training [24]. Concretely, a window with a fixed size W moves along the depth of the model, and the layers are partitioned into three disjoint regions: All layers preceding the window are used in an inference-only manner, with parameters frozen; All layers inside the window are trainable and receive gradient updates; All layers after the window are not yet included in the current network. This design focuses optimization on a small subset of layers at each step, improving computational efficiency and stabilizing the optimization dynamics. The detailed training process is given in Fig. 3.

Suppose that the sliding window now spans from the t_s^{th} layer to the t_e^{th} layer. The corresponding beamforming optimization problem is formulated as

$$\begin{aligned} \forall (K, N) \in [K_m] \times [N_m] : \\ \max_{\{\theta_t\}_{t=t_s}^{t_e}} \mathbb{E}_{\mathbf{H} \in \mathcal{S}^{K \times N}} \left[\sum_{t=t_s}^{t_e} R_{\text{sum}}(\mathbf{H}, \mathbf{W}^{(t)}) \right], \\ \text{s.t. } \|\mathbf{W}^{(t)}\|_F^2 \leq P, t \in [T]. \end{aligned} \quad (25)$$

Notably, the input pair to the trainable layers, namely $(\mathbf{H}^{(t_s-1)}, \mathbf{W}^{(t_s-1)})$, is generated by the first $(t_s - 1)$ layers, whose parameters are kept fixed during the current training stage. As the window slides across the entire architecture, every Transformer layer is progressively updated, ensuring that the full network is eventually trained without suffering from the instability caused by excessively long training horizons.

2) *Curriculum Learning with Random Masking*: Building upon the masked Transformer architecture introduced in Sec. III-B, we adopt a random masking strategy in this section to construct a diverse training dataset, thereby enhancing the robustness of the model to variations in both the number and identities of activated users and antennas. Specifically, given a Gaussian channel sample $\mathbf{H} \in \mathbb{C}^{K_m \times N_m}$ and the numbers of activated users and antennas (K, N) , we randomly mask out $(K_m - K)$ users and $(N_m - N)$ antennas by setting the corresponding rows and columns of \mathbf{H} to all-zero vectors.

Note that constructing a diverse training dataset requires frequent variation of the system parameters (K, N) during training. For clarity, we refer to each specific pair (K, N) as a *masking stage* or a *system configuration* in the sequel. We then

design a scheduling over (K, N) , which serves as a sample-based CL approach to improve the performance of this multi-stage training procedure. In particular, curriculum learning is a training paradigm in which neural networks are exposed to tasks of increasing difficulty, progressing from easier to harder ones. Such a strategy has been shown to mitigate premature convergence — an issue that is especially pronounced in large-scale system optimization problems with highly non-convex landscapes — by encouraging broader exploration of the solution space and acting as an implicit regularizer [12], [13].

Following the principle of CL, the model is initially trained on channel samples for which high-quality beamforming solutions are relatively easy to obtain, and the training progressively shifts toward more challenging channel realizations. As discussed in Sec. II-A, beamforming optimization generally becomes more difficult as the number of users increases, since the resulting IUI exhibits increasingly intricate coupling structures, thereby complicating effective interference suppression. Accordingly, we define a sequence of user numbers $\mathcal{K} = [K_1, \dots, K_U]$, along which the number of activated users K is gradually increased. For each fixed value of K , we further introduce an inner scheduling loop over the number of antennas by defining a sequence $\mathcal{N} = [N_1, \dots, N_V]$, along which N is varied sequentially. In practice, the sequences satisfy $0 < K_1 < \dots < K_U = K_m$ and $0 < N_1 < \dots < N_V = N_m$.

As a result, for each fixed trainable window spanning layers $[t_s, t_e]$ layers, a sample-based CL procedure is carried out by applying the scheduling of masking stages (K, N) and random masking operations. Specifically, for each masking stage $(K, N) \in \mathcal{K} \times \mathcal{N}$, $|\mathbf{R}_u| = K_m - K$, $|\mathbf{R}_a| = N_m - N$, and the masking matrices are generated based on the randomly-sampled index sets \mathbf{R}_u and \mathbf{R}_a . Notably, if the trainable window advances by one layer every T_w training epochs, and the masking stage transitions every T_m training epochs, then the two time scales are related by $T_w \triangleq |\mathcal{K}| \cdot |\mathcal{N}| \cdot T_m$.

3) *Sample Replay*: A potential issue of the multi-stage training scheme described in Sec. III-C2 is *model forgetting*, whereby performance on earlier stages may deteriorate as the model adapts to later stages [25]. To mitigate this effect, we incorporate a lightweight sample replay strategy [26]. Specifically, during training at each masking stage (K, N) , every mini-batch is composed of two parts: (i) a majority of samples drawn from the current masking stage, and (ii) a small fraction of replay samples randomly selected from previous stages. This replay mechanism helps preserve knowledge acquired in earlier stages, thereby maintaining performance consistency across stages and improving the overall robustness of the curriculum learning process.

Finally, the overall training and inference pipeline of the proposed model is summarized in Algorithm 1. Note that, although the multi-stage training procedure does not exhaustively traverse all possible masking stages (since $\mathcal{K} \subset [K_m]$ and $\mathcal{N} \subset [N_m]$), the resulting model is expected to generalize effectively to all configurations $(K, N) \in [K_m] \times [N_m]$ during inference.

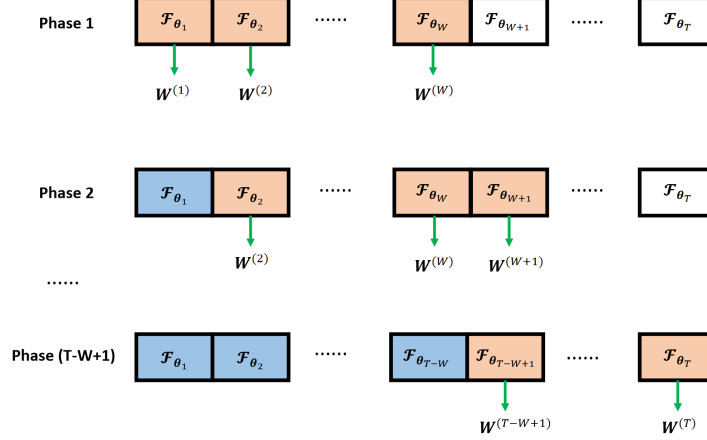


Fig. 3: Sliding-window training of the proposed model. A layer marked blue is in an inference-only manner, a layer marked red is in the trainable mode, and a layer marked white is not yet included in the network.

Algorithm 1 MT-SAO-lift model for dynamic multi-user downlink beamforming

- 1: **Parameters:** Sliding-window length W , sliding-window interval T_w , masking stage interval T_m , activated user schedule $\mathcal{K} = [K_1, \dots, K_U]$, activated antenna schedule $\mathcal{N} = [N_1, \dots, N_V]$
 - 2: Randomly initialize model parameters $\{\theta_t\}_{t=1}^T$, initialize the sliding-window as $[t_s, t_e] = [1, W]$, and initialize the masking stage as $(K_u, N_v) = (K_1, N_1)$
 - 3: **Training Phase:**
 - 4: **for** epoch $\ell = 1, 2, \dots$ **do**
 - 5: **if** $\ell \% T_w = 0$ **then**
 - 6: $t_s \leftarrow \min\{t_s + 1, T - W + 1\}$
 - 7: $t_e \leftarrow \min\{t_e + 1, T\}$
 - 8: $(K_u, N_v) \leftarrow (K_1, N_1)$
 - 9: **elseif** $\ell \% T_m = 0$ and $N_v < N_V$ **then**
 - 10: $(K_u, N_v) \leftarrow (K_u, N_{v+1})$
 - 11: **elseif** $\ell \% T_m = 0$ and $N_v = N_V$ **then**
 - 12: $(K_u, N_v) \leftarrow (K_{u+1}, N_1)$
 - 13: **end if**
 - 14: Obtain a training batch such that most samples are randomly masked with stage (K_u, N_v) , and a small fraction are replay samples from earlier stages
 - 15: Compute masking matrices by (12) and (16)
 - 16: Compute $\{\mathbf{W}^{(t)}\}_{t=t_s}^{t_e}$ according to Sec. III-B
 - 17: Update $\{\theta_t\}_{t=t_s}^{t_e}$ according to (25)
 - 18: **end for**
 - 19: **Output:** Trained model parameters $\{\theta_t^*\}_{t=1}^T$
 - 20: **Inference Phase:**
 - 21: Obtain a testing batch including randomly-masked samples covering all stages $(K, N) \in [K_m] \times [N_m]$
 - 22: Obtain the final solution $\mathbf{W}^{(T)}$ based on $\{\theta_t^*\}_{t=1}^T$
-

Table 1: Architecture of each Transformer network

Name	Notations	Size
FC layer	f_ℓ^s, f_ℓ^t	$40 \times 128 \times 2$
LN layer	$f_n^s, f_n^t, f_n^h, f_n^w$	128×4
Weight matrices	$\{\mathbf{Q}_s^e, \mathbf{K}_s^e, \mathbf{V}_s^e\}_{e=1}^E$	$128 \times 768 \times 12$
Weight matrices	$\{\mathbf{Q}_t^e, \mathbf{K}_t^e, \mathbf{V}_t^e\}_{e=1}^E$	$128 \times 768 \times 12$
Attention MLP	MLP_{sa}	138880
Output MLP	$\text{MLP}_h, \text{MLP}_w$	38400×2

D. Simulation Results

1) *Basic Settings:* We consider a single-cell downlink MISO system, where a BS equipped with $N_m = 40$ transmit antennas serves up to $K_m = 40$ single-antenna users within the cell. The Gaussian channel samples are generated according to (1). All users are assumed to experience identical noise variance, i.e., $\sigma_k^2 = \sigma^2$ for $\forall k \in [K]$. The transmit power is normalized such that $\|\mathbf{W}\|_F^2 = P = 1$, and the corresponding signal-to-noise ratio (SNR) is defined as $\text{SNR} = \frac{1}{\sigma^2}$.

Some basic parameters of Algorithm 1 are configured as follows. The activated user and antenna schedules are set to $\mathcal{K} = [8, 16, 24, 32, 40]$ and $\mathcal{N} = [8, 16, 24, 32, 40]$, respectively. The masking stage interval spans $T_m = 10$ training epochs, yielding the sliding-window interval $T_w = |\mathcal{K}| \cdot |\mathcal{N}| \cdot T_m = 250$ training epochs. The training batch size is $N_b^{(t)} = 128$, and the size of test dataset is $N_b^{(i)} = 80000$, i.e., 50 test samples for each configuration $(K, N) \in [K_m] \times [N_m]$. The learning rate is initialized as $\eta = 1 \times 10^{-4}$ and decayed to 3×10^{-5} following a cosine decay schedule. The step size of gradient ascent in (8) is set to $\eta_w = 10^{-2}$. The layer number of the MT-SAO-lift model is set to $T = 10$.

Moreover, Table 1 summarizes the parameter sizes of all components in the Transformer architecture shown in Fig. 2.

2) *Results:* We first evaluate the effectiveness of the proposed semi-amortized learning strategy by examining how the number of gradient ascent steps at each layer—denoted by Q_t during training and Q_i during inference—affects the final sum-rate performance. Specifically, three MT-SAO-lift mod-

els are trained with different training step numbers, namely $Q_t \in \{0, 5, 10\}$, and are subsequently evaluated under the system configuration $(K, N) = (40, 28)$ at SNR = 20 dB, while varying the inference step number Q_i . Fig. 4 plots the achieved sum rate as a function of Q_i for the three trained models. It can be observed that the model trained with $Q_t = 5$ significantly outperforms the one trained with $Q_t = 0$, demonstrating the effectiveness of the proposed semi-amortized design in producing high-quality beamformer solutions. Interestingly, the model with $Q_t = 5$ also outperforms that trained with $Q_t = 10$, indicating that an excessively large Q_t may aggravate the optimization difficulty and lead to inferior performance. During inference, employing a larger number of gradient ascent steps, i.e., $Q_i > Q_t$, further improves the achievable sum rate. Based on the results in Fig. 4, we set $Q_t = 5$ and $Q_i = 10$ for all subsequent simulations, which strikes a favorable balance between performance and computational complexity.

We next conduct an ablation study on the sliding-window training strategy described in Sec. III-C1. Specifically, three MT-SAO-lift models are trained using different sliding-window lengths W in Algorithm 1, and are evaluated on test samples generated under the system configuration $(K, N) = (40, 28)$. Fig. 5 plots the sum rate versus SNR for the three trained models, and compares their performances with the WMMSE and LMMSE baselines. It shows that the model with $W = 5$ outperforms the other two, indicating that an excessively large window size (e.g., $W = 10$) renders the end-to-end training more difficult, while an overly small window size (e.g., $W = 1$) fails to exploit the benefits of joint optimization across layers and thus limits the model expressivity. As a result, we adopt $W = 5$ for training in the subsequent simulations.

Next, we evaluate the testing performance of the proposed MT-SAO-lift model after fixing the key parameters. We begin by demonstrating that the masking operations endow the model with strong generalization capability. To this end, we introduce a baseline termed the dedicated-Transformer-based SAO-lift (DT-SAO-lift) model, which shares the same network architecture as the MT-SAO-lift model (except for masking components) but is trained and tested under a single system configuration (K, N) . Specifically, with SNR = 20dB and the number of activated antennas fixed at $N = 28$, Fig. 6 shows the sum rate versus the number of served users K using a single MT-SAO-lift model, and compares it with the performance of DT-SAO-lift models individually trained for each value of K . It is seen that the generalizable MT-SAO-lift model consistently outperforms or approaches the performance of the DT-SAO-lift models across all regimes, including both underloaded and overloaded cases, while avoiding the substantial retraining overhead under varying configurations. Note that, the MT-SAO-lift model also exhibits strong performance on test samples corresponding to unseen system configurations $(K, N) \in [K_m] \times [N_m]$ during training, highlighting its ability to interpolate across unseen combinations within the training distribution. Furthermore, the performance gap between the WMMSE and LMMSE baselines becomes increasingly pronounced as K grows, revealing why learning becomes

more challenging and convergence slows down in overloaded regimes — the proposed scheme adopts the LMMSE beamformer as the initialization, which provides a less favorable starting point in overloaded systems. In addition, interference suppression becomes intrinsically more difficult when the number of served users exceeds the number of transmit antennas.

We further compare the performance of the two proposed models introduced in Remark 1, namely the MT-SAO-lift model and the masked-Transformer-based SAO (MT-SAO) model. Specifically, with SNR = 20dB and $K = 40$ fixed, Fig. 7 depicts the sum rate versus the number of activated antennas N for both models. It shows that the MT-SAO-lift model consistently outperforms the MT-SAO model, indicating that updating the auxiliary variables at each layer, which act as a representation lifting, enhances the model's expressive power and leads to higher-quality beamformer solutions. Moreover, the advantage of the MT-SAO-lift model becomes more evident in heavily-overloaded regimes. In contrast, under critically-loaded or underloaded conditions, the performance of the MT-SAO model closely approaches that of the MT-SAO-lift model. This observation motivates the introduction of the MT-SAO model: it can serve as a lower-complexity alternative to the MT-SAO-lift model in underloaded scenarios, where the benefit of representation lifting is marginal. Nevertheless, the MT-SAO-lift model remains indispensable for achieving high-quality beamforming solutions across the full range of system configurations, particularly in overloaded settings.

Finally, we compare the proposed MT-SAO-lift model with several existing baseline methods, summarized as follows:

- **WMMSE:** The classical iterative beamforming optimization algorithm [1].
- **Graph Transformer:** A Transformer model that emulates GNN training over heterogeneous graphs, exhibiting improved size-generalizability [27].
- **HPE Transformer:** A WMMSE-guided, Transformer-based multi-layer beamforming scheme [14].
- **LLM-adapter:** A precoding framework based on a pre-trained GPT-2 model with task-specific adapters designed for various system scenarios [28].
- **RNN Optimizer:** An online gradient-based recurrent optimization scheme [15].

Fig. 8 illustrates the sum rate versus the number of served users K for different beamforming schemes, with $N = 28$ and SNR = 20dB. To ensure a fair comparison, except for the WMMSE algorithm baseline [1] and the online optimization baseline [15], all other learning-based schemes are trained using the CL-based sample scheduling in Sec. III-C2 (without sliding-window training method) until convergence. As observed in Fig. 8, the proposed MT-SAO-lift scheme consistently outperforms all competing learning-based methods. In addition, all Transformer-based schemes can approach or surpass the WMMSE baseline in the underloaded systems; However, in overloaded regimes, all baselines incur the performance degradations compared with the WMMSE algorithm, whereas the proposed scheme maintains performance compa-

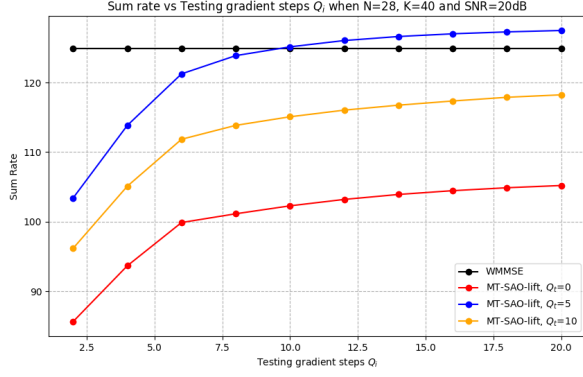


Fig. 4: Performance under different numbers of gradient steps during training (Q_t) and testing (Q_i).

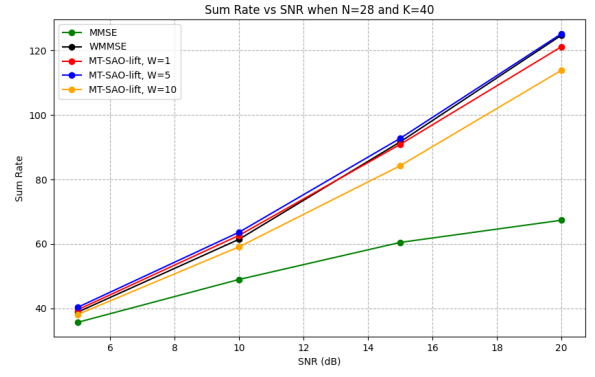


Fig. 5: Performance under different sliding-window lengths.

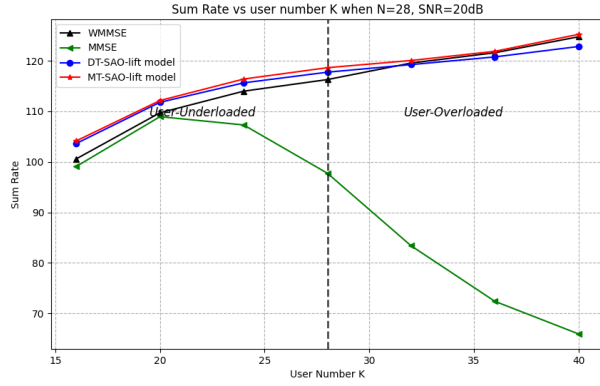


Fig. 6: Performance comparison between a single MT-SAO-lift model and multiple DT-SAO-lift models.

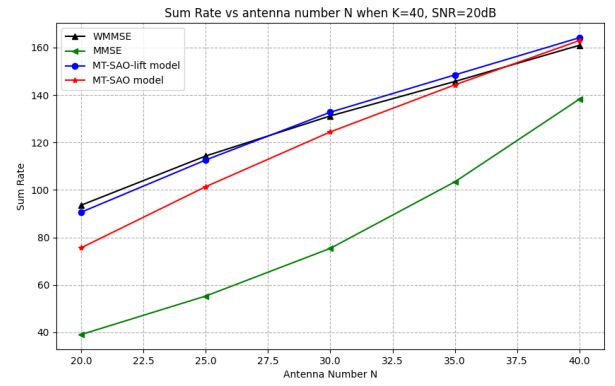


Fig. 7: Performance comparison between a MT-SAO-lift model and a MT-SAO model.

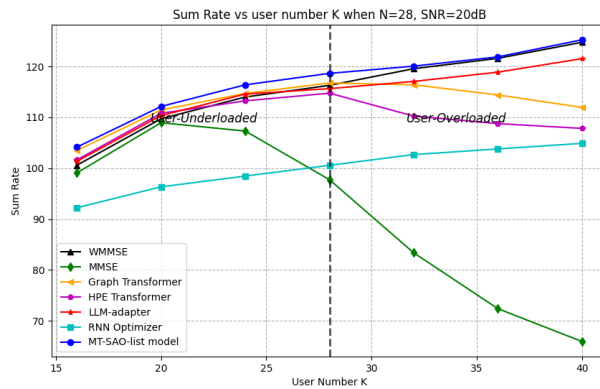


Fig. 8: Comparison between the proposed scheme and several baseline methods.

erable to that of WMMSE.

We further report in Table 2 the average CPU inference time of all schemes with a batch size of 100 under the system configuration $(K, N) = (40, 40)$. The results show that the proposed model achieves a faster inference speed than

the WMMSE algorithm, the online RNN scheme, and the heavyweight LLM-adaptor scheme, but is slower than other Transformer-based methods in [14], [27] due to the additional steps of gradient ascent during inference.

IV. APPLICATIONS TO INTEGRATED SENSING AND COMMUNICATION SYSTEMS

In this section, we show that our proposed Transformer-based SAO framework can be extended to ISAC applications. To jointly enhance both sensing and communication performance, we develop a joint radar-communication beamforming (JRCB) scheme, in which the transmit signal is designed as a weighted superposition of communication symbols and radar waveforms [29].

A. System Description and Problem Formulation

1) *System Description:* Consider an ISAC system in which a BS simultaneously functions as a mono-static MIMO radar and a downlink MU-MISO communication transmitter. The BS, equipped with N antennas, operates in the TDD mode to serve K single-antenna users while sensing M randomly distributed point-like targets. The communication channel is modeled as a Gaussian-sampled random matrix, where each

Table 2: Inference time per batch (batch size 100, 20dB, 40×40 channels).

Scheme	WMMSE	RNN	LLM-adapter	MT-SAO-lift model	Graph Transformer	HPE Transformer
Time (s)	8.782	5.34	0.148	0.042	0.026	0.018

realization $\mathbf{H} \in \mathbb{C}^{K \times N}$ has independent entries drawn according to (1). For the sensing channel, we consider a monostatic MIMO radar deployed at the BS, where the transmitted waveform is reflected by multiple single-point targets. Under a single-path assumption for each target's reflected channel, the sensing channel is modeled as

$$\mathbf{G} = \sum_{m=1}^M \mathbf{G}_m = \sum_{m=1}^M \beta_m \mathbf{a}_r(\theta_m) \mathbf{a}_t^H(\theta_m) \in \mathbb{C}^{N \times N}, \quad (26)$$

where $\beta_m \sim \mathcal{CN}(0, 1)$, $\forall m \in [M]$, denotes the composite sensing channel gain of the m^{th} target, accounting for path-loss and radar cross section (RCS), and $\mathbf{a}_r(\theta_m)$ and $\mathbf{a}_t(\theta_m)$ are the corresponding receive and transmit array response vectors, respectively. In this work, we focus on joint beamforming optimization, assuming that the both the communication channel $\mathbf{H} \in \mathbb{C}^{K \times N}$ and the sensing channel $\mathbf{G} \in \mathbb{C}^{N \times N}$ are perfectly known at the BS.

Let the transmit signal of the BS at the ℓ^{th} time slot be expressed as $\mathbf{x}[\ell] = \mathbf{W} \cdot \mathbf{c}[\ell] + \mathbf{F} \cdot \mathbf{s}[\ell]$, $\ell \in [L]$, where $\mathbf{W} \in \mathbb{C}^{N \times K}$ denotes the communication beamformer satisfying $\|\mathbf{W}\|_F^2 = P_c$, and $\mathbf{F} \in \mathbb{C}^{N \times N}$ represents the sensing beamformer satisfying $\|\mathbf{F}\|_F^2 = P_s$. The vector $\mathbf{c}[\ell] = [c_1[\ell], \dots, c_K[\ell]]^T \in \mathbb{C}^K$ contains the communication symbols for K users, with $\mathbb{E}(\mathbf{c}[\ell] \mathbf{c}^H[\ell]) = \mathbf{I}_K$. Similarly, $\mathbf{s}[\ell] \in \mathbb{C}^N$ denotes the radar waveform, satisfying $\mathbb{E}(\mathbf{s}[\ell] \mathbf{s}^H[\ell]) = \mathbf{I}_N$. The communication and radar symbols are assumed to be mutually uncorrelated, i.e., $\mathbb{E}(\mathbf{s}[\ell] \mathbf{c}^H[\ell]) = \mathbf{0}_{N \times K}$.

2) *Problem Formulation*: It has been shown in [30] that, under the assumption of well-separated targets in large-scale multiple-input-multiple-output (MIMO) systems, the sensing SNR of each target provides a reliable surrogate metric for radar binary detection performance. Moreover, since the communication signal is known at the radar receiver in monostatic ISAC systems, it can be coherently exploited to enhance the sensing SNR. Specifically, the sensing SNR associated with the m -th target can be expressed as

$$\begin{aligned} \text{SNR}_m^s &= \frac{\mathbb{E}\{\|\mathbf{G}_m(\mathbf{W}\mathbf{c}[\ell] + \mathbf{F}\mathbf{s}[\ell])\|^2\}}{\sigma_z^2} \\ &= \frac{\|\mathbf{G}_m \mathbf{W}\|_F^2 + \|\mathbf{G}_m \mathbf{F}\|_F^2}{\sigma_z^2}, \end{aligned} \quad (27)$$

In contrast, from the perspective of the communication users, the sensing signal acts as interference, since it is unknown at their receivers. Let $\mathbf{h}_k \in \mathbb{C}^{N \times 1}$ and $\mathbf{w}_k \in \mathbb{C}^{N \times 1}$ denote the downlink channel vector and the corresponding beamforming vector from the BS to the k -th user, respectively. The received signal-to-interference-ratio (SINR) of the k -th user is then given by

$$\text{SINR}_k^c = \frac{|\mathbf{h}_k^H \mathbf{w}_k|^2}{\sum_{i \neq k} |\mathbf{h}_k^H \mathbf{w}_i|^2 + \|\mathbf{h}_k \mathbf{F}\|^2 + 1}, \quad (28)$$

where the second term in the denominator captures the interference induced by the sensing signal. In principle, this interference can be mitigated by projecting the sensing beamformer \mathbf{F} onto the null space of the communication channel matrix \mathbf{H} , i.e., enforcing $\mathbf{H}^H \mathbf{F} \approx \mathbf{0}$.

In this work, we adopt a communication-centric ISAC optimization framework that aims to maximize the achievable communication sum rate while guaranteeing a minimum sensing quality for all targets. In addition, the joint beamforming design is subject to a total transmit power constraint at the BS. Accordingly, the optimization problem is formulated as

$$\max_{\mathbf{W}, \mathbf{F}} R_{\text{sum}} = \sum_{k=1}^K \log(1 + \text{SINR}_k^c), \quad (29a)$$

$$\text{s.t.} \quad \text{SNR}_m^s \geq \gamma_s, \quad \forall m \in [M], \quad (29b)$$

$$\|\mathbf{W}\|_F^2 + \|\mathbf{F}\|_F^2 \leq P_0, \quad (29c)$$

where SINR_k^c and SNR_m^s are defined in (28) and (27), respectively. It is noteworthy that the power allocations between the communication and sensing beamformers, namely (P_c, P_s) , can be further optimized to achieve a desirable trade-off between communication throughput and sensing performance.

We next reformulate the optimization problem in (29) to make it compatible with the proposed SAO framework introduced in Sec. III-A. To handle the total power constraint in (29c), we explicitly enforce $\|\mathbf{W}\|_F^2 = P_c$ and $\|\mathbf{F}\|_F^2 = P_s$, with $P_c + P_s \leq P_0$, where P_c and P_s are treated as learnable parameters. To incorporate the sensing SNR constraint in (29b), we adopt a differentiable log-barrier function [31], which imposes an increasingly strong penalty as the constraint boundary is approached. This technique enables the construction of an unconstrained loss function while maintaining feasibility. The resulting layer-wise loss function is given by

$$\begin{aligned} \mathcal{H}(\mathbf{W}^{(t)}, \mathbf{F}^{(t)}; \mathbf{H}, \{\mathbf{G}_m\}_{m=1}^M) &= R_{\text{sum}}(\mathbf{H}, \mathbf{W}^{(t)}, \mathbf{F}^{(t)}) \\ &\quad - \lambda_s \cdot \sum_{m=1}^M \log\left(\text{SNR}_m^s(\mathbf{W}^{(t)}, \mathbf{F}^{(t)}; \mathbf{G}_m) - \gamma_s\right), \end{aligned} \quad (30)$$

where $\mathbf{W}^{(t)}$ and $\mathbf{F}^{(t)}$ denote the communication and sensing beamformers produced at the t^{th} layer, respectively. Assume that $\mathbf{H} \in \mathcal{S}^{K \times N}$ and $\mathbf{G}_m \in \mathcal{T}^{N \times N}$ for all $m \in [M]$. Similar to (25), let θ_t denote the learnable parameters of the optimizer networks at the t^{th} layer, and the sliding-window training method in Sec. III-C1 is employed. Based on the loss function in (30), the amortized joint beamforming optimization problem is as follows,

$$\begin{aligned} \min_{\{\theta_t\}_{t=t_s}^{t_e}} \mathbb{E}_{\mathbf{H} \in \mathcal{S}^{K \times N}, \mathbf{G}_m \in \mathcal{T}^{N \times N}} \left[\sum_{t=t_s}^{t_e} \mathcal{H}(\mathbf{W}^{(t)}, \mathbf{F}^{(t)}; \mathbf{H}, \{\mathbf{G}_m\}_{m=1}^M) \right], \\ \text{s.t.} \quad \|\mathbf{W}\|_F^2 = P_c, \quad \|\mathbf{F}\|_F^2 = P_s, \quad P_c + P_s \leq P_0, \end{aligned} \quad (31)$$

where t_s and t_e denote the indices of the first and last trainable layers, respectively.

B. SAO-ISAC Model for ISAC System Optimization

Inspired by the SAO framework in Sec. III-A, we develop in this section an SAO-for-ISAC (SAO-ISAC) model tailored to the joint optimization problem in (31). The overall architecture of the proposed SAO-ISAC model is depicted in Fig. 9. We initialize $\mathbf{H}^{(0)} = \mathbf{H}$ and $\mathbf{G}^{(0)} = \mathbf{G}$. The communication beamformer $\mathbf{W}^{(0)}$ is initialized as the LMMSE beamformer of \mathbf{H} , whereas the initial sensing beamformer $\mathbf{F}^{(0)}$ is constructed by projecting onto the null space of the communication channel \mathbf{H} .

The SAO-ISAC model is organized in a layered manner. Specifically, the t^{th} layer consists of a communication block $\text{CB}_{\theta_t^c}$ and a sensing block $\text{SB}_{\theta_t^s}$, whose parameter sets satisfy $\theta_t^c \cup \theta_t^s = \theta_t$. Note that the power allocation variables P_c and P_s are included in θ_t^c and θ_t^s , respectively. At the t^{th} layer, the auxiliary feature $\mathbf{H}^{(t-1)}$ together with the previous communication beamformer $\mathbf{W}^{(t-1)}$ is fed into the communication block $\text{CB}_{\theta_t^c}$, whereas the auxiliary feature $\mathbf{G}^{(t-1)}$ and the previous sensing beamformer $\mathbf{F}^{(t-1)}$ are provided as inputs to the sensing block $\text{SB}_{\theta_t^s}$. Similar to the update rule in (10), the communication block $\text{CB}_{\theta_t^c}$ first produces the following outputs:

$$\begin{aligned} \mathbf{H}^{(t)} &= \mathbf{H}^{(t-1)} + \text{CB}_{\theta_t^c}(\mathbf{H}^{(t-1)}, \mathbf{W}^{(t-1)})[0], \\ \mathbf{W}_0^{(t)} &= \mathbf{W}^{(t-1)} + \text{CB}_{\theta_t^c}(\mathbf{H}^{(t-1)}, \mathbf{W}^{(t-1)})[1], \end{aligned} \quad (32)$$

and then obtains the refined communication beamformer $\mathbf{W}^{(t)} \triangleq \mathbf{W}_Q^{(t)}$ as follows

$$\begin{aligned} \mathbf{W}_q^{(t)} &= \mathbf{W}_{q-1}^{(t)} + \eta_w \cdot \nabla_{\mathbf{W}} R_{\text{sum}}(\mathbf{W}_{q-1}^{(t)}, \mathbf{F}^{(t-1)}; \mathbf{H}), \\ \mathbf{W}_q^{(t)} &= \sqrt{P_c} \cdot \frac{\mathbf{W}_q^{(t)}}{\|\mathbf{W}_q^{(t)}\|_F}, \quad q \in [Q]. \end{aligned} \quad (33)$$

Similarly, the sensing block $\text{SB}_{\theta_t^s}$ first outputs

$$\begin{aligned} \mathbf{G}^{(t)} &= \mathbf{G}^{(t-1)} + \text{SB}_{\theta_t^s}(\mathbf{G}^{(t-1)}, \mathbf{F}^{(t-1)})[0], \\ \mathbf{F}_0^{(t)} &= \mathbf{F}^{(t-1)} + \text{SB}_{\theta_t^s}(\mathbf{G}^{(t-1)}, \mathbf{F}^{(t-1)})[1]. \end{aligned} \quad (34)$$

and then obtains the refined sensing beamformer solution $\mathbf{F}^{(t)} \triangleq \mathbf{F}_Q^{(t)}$ as follows

$$\begin{aligned} \mathbf{F}_q^{(t)} &= \mathbf{F}_{q-1}^{(t)} + \eta_f \cdot \nabla_{\mathbf{F}} \left[\sum_{m=1}^M \log \left(\right. \right. \\ &\quad \left. \left. \text{SNR}_m^s(\mathbf{W}^{(t)}, \mathbf{F}_{q-1}^{(t)}; \mathbf{G}_m) - \gamma \right) \right], \\ \mathbf{F}_q^{(t)} &= \sqrt{P_s} \cdot \frac{\mathbf{F}_q^{(t)}}{\|\mathbf{F}_q^{(t)}\|_F}, \quad q \in [Q]. \end{aligned} \quad (35)$$

Consequently, the updated beamformer solutions $\mathbf{W}^{(t)}$ and $\mathbf{F}^{(t)}$ are obtained at the t^{th} layer. The combined loss function in (30) is then evaluated, and gradient backpropagation is performed to jointly optimize the learnable parameters of the communication and sensing blocks. The overall training and inference procedures of the proposed SAO-ISAC model are summarized in Algorithm 2.

Algorithm 2 Transformer-based SAO-ISAC model for joint beamforming in ISAC systems

- 1: **Parameters:** Sliding-window length W , sliding-window interval T_w
 - 2: Randomly initialize model parameters $\{\theta_t\}_{t=1}^T$, initialize the sliding window as $[t_s, t_e] = [1, W]$
 - 3: **Training Phase:**
 - 4: **for** epoch $\ell = 1, 2, \dots$ **do**
 - 5: **if** $\ell \% T_w = 0$ **then**
 - 6: $t_s \leftarrow \min\{t_s + 1, T - W + 1\}$
 - 7: $t_e \leftarrow \min\{t_e + 1, T\}$
 - 8: Obtain a training batch of communication and sensing channels by (1) and (26)
 - 9: Obtain the initial communication and sensing beamformers $\mathbf{W}^{(0)}$ and $\mathbf{F}^{(0)}$
 - 10: Obtain $\{(\mathbf{W}^{(t)}, \mathbf{F}^{(t)})\}_{t=t_s}^{t_e}$ by (32) - (35)
 - 11: Update $\{\theta_t\}_{t=t_s}^{t_e}$ based on (31)
 - 12: **end for**
 - 13: **Output:** Trained model parameters $\{\theta_t^*\}_{t=1}^T$
 - 14: **Inference Phase:**
 - 15: Obtain a testing batch of channels
 - 16: Obtain final solutions $(\mathbf{W}^{(T)}, \mathbf{F}^{(T)})$ based on $\{\theta_t^*\}_{t=1}^T$
-

Another well-established ISAC formulation considers joint beamforming optimization that simultaneously maximizes the communication rate and the sensing rate [32]. The proposed Transformer-based SAO-ISAC model can be readily extended to this formulation by adopting a weighted sum of the communication rate and sensing rate as the learning objective in (31).

C. Simulation Results

1) *Basic Settings:* We set the number of transmit antennas at the BS to $N = 32$, the number of communication users to $K = 32$, and the number of sensing targets to $M = 5$. The total transmit power is fixed as $P_0 = P_c + P_s = 1$. The communication SNR for each user is defined as $\text{SNR}_c^c = \frac{P_c}{\sigma_z^2}$, while the radar receiver noise variance is $\sigma_z^2 = 0.01$. We directly adopt the parameter settings in Sec. III-D. In particular, the proposed SAO-ISAC model consists of $T = 10$ Transformer-based layers, with $Q_t = 5$ gradient ascent steps following each block during training and $Q_i = 10$ steps during inference. The sliding-window length is set to $W = 5$. For each $m \in [M]$, the sensing target angle θ_m in (26) is randomly drawn from the interval $[0, \frac{\pi}{2}]$. The weighting coefficient λ_s in (30) is set to 1.

2) *Results:* We now evaluate the impact of the sensing components on communication performance. Specifically, we examine the achieved communication rates under varying numbers of sensing targets M and different sensing SNR thresholds γ_s . Note that the training loss function in (30) does not strictly enforce feasibility, i.e., the constraint in (29b) may not be satisfied for every sensing target in all realizations. Therefore, in addition to communication performance, we also assess the feasibility probability of the sensing beamformers across the test set. The communication SNR is fixed at 15dB. Fig. 10a and Fig. 10b show the sum rate and the feasibility

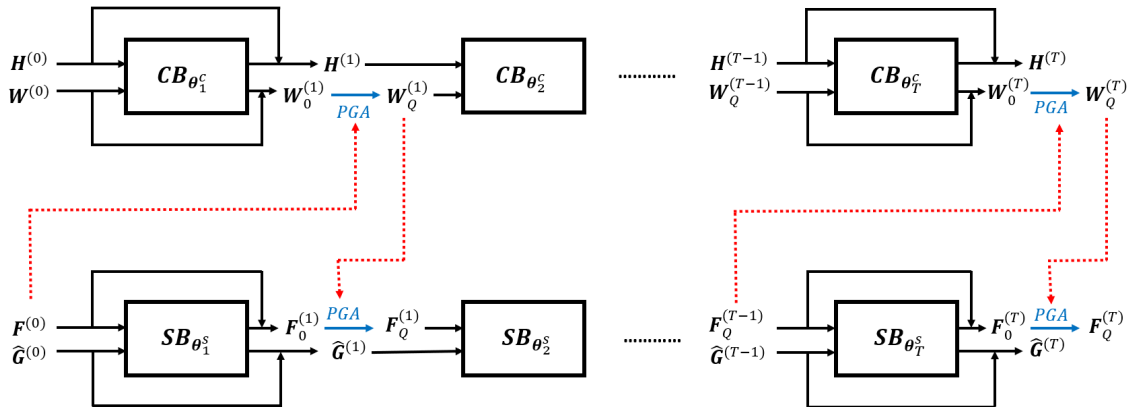


Fig. 9: Block diagram of the proposed SAO-ISAC model.

probability versus M under different values of γ_s , respectively. It can be observed that, as the number of sensing targets increases and the sensing SNR threshold becomes more stringent, the communication sum rate decreases and the sensing feasibility probability declines. These results reveal a clear trade-off between achieving higher communication throughput and maintaining accurate sensing performance when serving more targets.

Finally, we compare the proposed SAO-ISAC scheme with the following existing baseline methods, summarized as follows:

- **LMMSE+Null-space:** The LMMSE solution is applied as the communication beamformer, while the sensing beamformer is obtained by projecting onto the null space of the communication channel. This approach is simple to implement but provides limited performance in both communication rate and sensing accuracy.
- **SDP:** The problem in (29) is formulated as a semidefinite program (SDP) and solved using convex solvers. The solution of the relaxed problem is then mapped back to the original problem space, as analyzed in [33]. The major drawback of this method is its high computational complexity.
- **DNN:** Three DNNs are employed to alternately optimize the communication beamformers, sensing beamformers, and power allocations based on (29). This scheme was proposed in [30], but it was not evaluated under large-scale user or sensing target scenarios in that work.

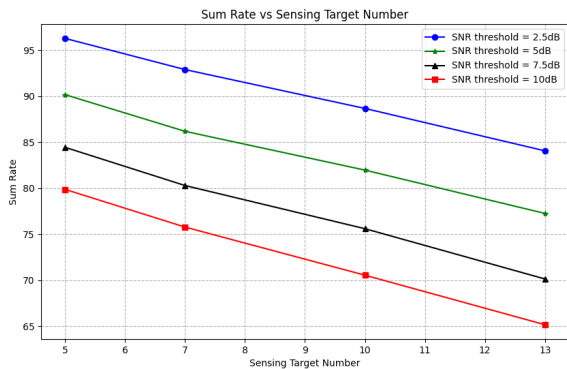
Figs. 11a and 11b illustrate the testing communication sum rate and the feasibility probability versus communication SNR for different ISAC beamforming schemes, respectively, with $N = K = 32$, $M = 5$ and $\gamma_s = 5\text{dB}$. It can be observed that the communication rate increases with higher communication SNR, and the proposed scheme consistently outperforms all baseline methods across the entire SNR range. Moreover, the feasibility probability of the proposed scheme is either higher than or comparable to that of the ‘‘DNN’’ baseline at all SNR levels, and significantly exceeds those of the ‘‘SDP’’ and ‘‘LMMSE+Null-space’’ baselines.

V. CONCLUSIONS

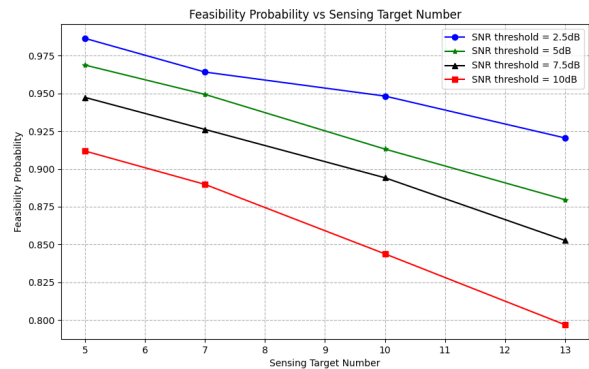
The proposed multi-layer Transformer model enables real-time downlink beamforming over large-scale channels. Simulation results show that it consistently outperforms all baseline methods, including the WMMSE algorithm, while achieving the lowest inference time per channel sample. Moreover, the model generalizes well to larger channel dimensions and higher SNR regimes. Future work will extend this framework to sparse channels with even larger dimensions and explore sparsity-aware design strategies.

REFERENCES

- [1] Q. Shi, M. Razaviyayn, Z.-Q. Luo, and C. He, ‘‘An iteratively weighted mmse approach to distributed sum-utility maximization for a mimo interfering broadcast channel,’’ *IEEE Transactions on Signal Processing*, vol. 59, no. 9, pp. 4331–4340, 2011.
- [2] A. Lozano, A. M. Tulino, and S. Verdu, ‘‘Optimum power allocation for parallel gaussian channels with arbitrary input distributions,’’ *IEEE Transactions on Information Theory*, vol. 52, no. 7, pp. 3033–3051, 2006.
- [3] E. Bjornson, M. Bengtsson, and B. Ottersten, ‘‘Optimal multiuser transmit beamforming: A difficult problem with a simple solution structure [lecture notes],’’ *IEEE Signal Processing Magazine*, vol. 31, no. 4, pp. 142–148, 2014.
- [4] W. Xia, G. Zheng, Y. Zhu, J. Zhang, J. Wang, and A. P. Petropulu, ‘‘A deep learning framework for optimization of miso downlink beamforming,’’ *IEEE Transactions on Communications*, vol. 68, no. 3, pp. 1866–1880, 2019.
- [5] C. Liu, W. Yuan, S. Li, X. Liu, H. Li, D. W. K. Ng, and Y. Li, ‘‘Learning-based predictive beamforming for integrated sensing and communication in vehicular networks,’’ *IEEE Journal on Selected Areas in Communications*, vol. 40, no. 8, pp. 2317–2334, 2022.
- [6] Y. Cui, J. Nie, X. Cao, T. Yu, J. Zou, J. Mu, and X. Jing, ‘‘Sensing-assisted high reliable communication: A transformer-based beamforming approach,’’ *IEEE Journal of Selected Topics in Signal Processing*, vol. 18, no. 5, pp. 782–795, 2024.
- [7] Y. Zhang, J. Johnston, and X. Wang, ‘‘An encoder-decoder network for beamforming over sparse large-scale mimo channels,’’ *arXiv preprint arXiv:2510.02355*, 2025.
- [8] Y. Zhang, S. Li, D. Li, J. Zhu, and Q. Guan, ‘‘Transformer-based predictive beamforming for integrated sensing and communication in vehicular networks,’’ *IEEE Internet of Things Journal*, vol. 11, no. 11, pp. 20 690–20 705, 2024.
- [9] H. Ting, Z. Wang, and Y. Liu, ‘‘Adaptive ttd configurations for near-field communications: An unsupervised transformer approach,’’ *IEEE Transactions on Wireless Communications*, 2024.
- [10] L. Pellaco, M. Bengtsson, and J. Jalden, ‘‘Deep unfolding of the weighted mmse beamforming algorithm,’’ *arXiv preprint arXiv:2006.08448*, 2020.

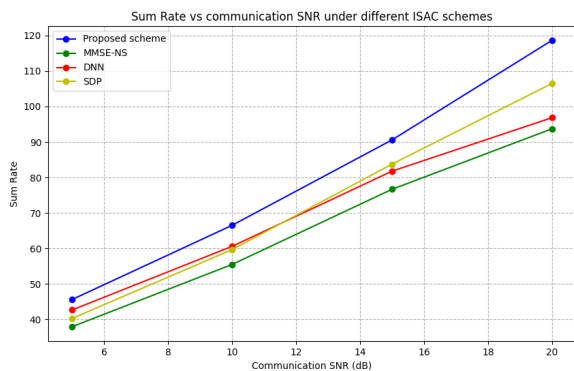


(a) Sum rate performance.

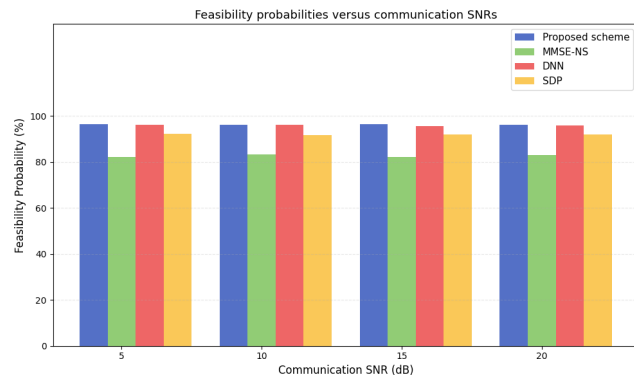


(b) Feasibility probability performance.

Fig. 10: ISAC performance under different numbers of sensing targets and different sensing SNR thresholds.



(a) Sum rate performance.



(b) Feasibility probability performance.

Fig. 11: Comparison between the proposed scheme and several ISAC joint beamforming baselines.

- [11] T. Chen, X. Chen, W. Chen, H. Heaton, J. Liu, Z. Wang, and W. Yin, "Learning to optimize: A primer and a benchmark," *Journal of Machine Learning Research*, vol. 23, no. 189, pp. 1–59, 2022.
- [12] Y. Bengio, J. Louradour, R. Collobert, and J. Weston, "Curriculum learning," in *Proceedings of the 26th annual international conference on machine learning*, 2009, pp. 41–48.
- [13] J. Johnston, X.-Y. Liu, S. Wu, and X. Wang, "A curriculum learning approach to optimization with application to downlink beamforming," *IEEE Transactions on Signal Processing*, 2023.
- [14] Y. Li and Y.-F. Liu, "Hpe transformer: Learning to optimize multi-group multicast beamforming under nonconvex qos constraints," *IEEE Transactions on Communications*, vol. 72, no. 9, pp. 5581–5594, 2024.
- [15] J. Johnston and X. Wang, "Rnn beamforming optimizer for rate-splitting multiple access and cell-free massive mimo," *IEEE Transactions on Communications*, 2024.
- [16] B. Amos *et al.*, "Tutorial on amortized optimization," *Foundations and Trends® in Machine Learning*, vol. 16, no. 5, pp. 592–732, 2023.
- [17] N. Rajapaksha, J. Mohammadi, S. Wesemann, T. Wild, and N. Rajatheva, "Minimizing energy consumption under non-mimo via antenna muting by neural networks with asymmetric loss," *IEEE Transactions on Vehicular Technology*, vol. 73, no. 5, pp. 6600–6613, 2023.
- [18] H. Joudeh and B. Clerckx, "Rate-splitting for max-min fair multigroup multicast beamforming in overloaded systems," *IEEE Transactions on Wireless Communications*, vol. 16, no. 11, pp. 7276–7289, 2017.
- [19] Y. Kim, S. Wiseman, A. Miller, D. Sontag, and A. Rush, "Semi-amortized variational autoencoders," in *International Conference on Machine Learning*. PMLR, 2018, pp. 2678–2687.
- [20] K. He, X. Zhang, S. Ren, and J. Sun, "Deep residual learning for image recognition," in *Proceedings of the IEEE conference on computer vision and pattern recognition*, 2016, pp. 770–778.
- [21] H. Zhou, A. Bradley, E. Littwin, N. Razin, O. Saremi, J. Susskind, S. Bengio, and P. Nakkiran, "What algorithms can transformers learn? a study in length generalization," *arXiv preprint arXiv:2310.16028*, 2023.
- [22] B. Cheng, I. Misra, A. G. Schwing, A. Kirillov, and R. Girdhar, "Masked-attention mask transformer for universal image segmentation," in *Proceedings of the IEEE/CVF conference on computer vision and pattern recognition*, 2022, pp. 1290–1299.
- [23] Z. Fan, Y. Gong, D. Liu, Z. Wei, S. Wang, J. Jiao, N. Duan, R. Zhang, and X. Huang, "Mask attention networks: Rethinking and strengthen transformer," 2021. [Online]. Available: <https://arxiv.org/abs/2103.13597>
- [24] C. Tallec and Y. Ollivier, "Unbiasing truncated backpropagation through time," *arXiv preprint arXiv:1705.08209*, 2017.
- [25] M. Toneva, A. Sordoni, R. T. d. Combes, A. Trischler, Y. Bengio, and G. J. Gordon, "An empirical study of example forgetting during deep neural network learning," *arXiv preprint arXiv:1812.05159*, 2018.
- [26] D. Rolnick, A. Ahuja, J. Schwarz, T. P. Lillicrap, and G. Wayne, "Experience replay for continual learning," 2019. [Online]. Available: <https://arxiv.org/abs/1811.11682>
- [27] Y. Duan, J. Guo, and C. Yang, "Learning precoding in multi-user multi-antenna systems: Transformer or graph transformer?" *arXiv preprint arXiv:2503.02998*, 2025.
- [28] Z. Xu, T. Zheng, and L. Dai, "Llm-empowered near-field communications for low-altitude economy," *IEEE Transactions on Communications*, 2025.
- [29] X. Liu, T. Huang, N. Shlezinger, Y. Liu, J. Zhou, and Y. C. Eldar, "Joint transmit beamforming for multiuser mimo communications and mimo radar," *IEEE Transactions on Signal Processing*, vol. 68, pp. 3929–3944, 2020.
- [30] R. Yang, Z. Zhu, J. Zhang, S. Xu, C. Li, Y. Huang, and L. Yang, "Deep learning-based joint transmit beamforming for dual-functional radar-communication system," *IEEE Transactions on Wireless Communications*, 2024.

- [31] S. Boyd and L. Vandenberghe, *Convex optimization*. Cambridge university press, 2004.
- [32] C. Ouyang, Y. Liu, and H. Yang, "On the performance of uplink isac systems," *IEEE Communications Letters*, vol. 26, no. 8, pp. 1769–1773, 2022.
- [33] U. Demirhan and A. Alkhateeb, "Cell-free isac mimo systems: Joint sensing and communication beamforming," *IEEE Transactions on Communications*, 2024.